International Journal of Heat and Mass Transfer 66 (2013) 613–624

Contents lists available at ScienceDirect

International Journal of Heat and Mass Transfer

journal homepage: www.elsevier.com/locate/ijhmt

Effect of nanotextured array of conical features on explosive boiling over a flat substrate: A nonequilibrium molecular dynamics study

Hamid Reza Seyf, Yuwen Zhang *

Department of Mechanical and Aerospace Engineering, University of Missouri, Columbia, MO 65211, USA

ARTICLE INFO

Article history:
Received 2 April 2013
Received in revised form 3 July 2013
Accepted 6 July 2013
Available online 16 August 2013

Keywords:
Nanostructure
Molecular dynamics simulation
Boiling
Nanocone array

ABSTRACT

Nonequilibrium molecular dynamics simulations were performed to investigate the effects of size of nanocone array and types of wall material, i.e., aluminum and silver, on the explosive boiling of ultra-thin liquid argon film on nanostructure. An Embedded Atom Method (EAM) potential is used in describing the interatomic interaction between metal atoms. The results showed that the cone-like nanostructures drastically enhance heat transfer from solid to liquid and they have significant effects on temperature and pressure histories, net evaporation number, as well as the density distribution in the system. In all cases studied, the liquid molecules above the solid surface go into explosive boiling and a cluster of liquid is observed to move upward. It was also observed that the separation temperature associated with separation of liquid film from solid surface strongly depends on size of nanostructure while it is not sensitive to the type of materials. Furthermore, in all cases in a specific time after beginning of boiling, the evaporation on the hot wall stopped and a non-evaporating layer will form on the surface.

1. Introduction

Boiling is an important phase change phenomenon that occurs in variety of applications such as electronic cooling, power generation, refrigeration, and cryogenics. It is defined as the process of phase change from liquid to vapor by heating the liquid past its saturation temperature and is characterized by nucleation, growth and detachment of the vapor bubbles. Explosive boiling [1] is a special kind of boiling that the phase transition from liquid to vapor occurs very rapidly. In this process the liquid is heated far beyond its saturation temperature so the phase transition from liquid to vapor is accompanied by a sharp pressure increase. It is encountered in nuclear and chemical industries and various emerging technologies such as ultra-fast laser materials processing. Although a large number of experimental and numerical investigations have been performed over the last decades [2–11], this phenomenon is still one of the least understood topics in heat transfer. Therefore, no well-established theory exists for predicting the rate of heat transfer in explosive boiling. However, due to practical importance of heat transfer in explosive boiling, researchers have proposed various phenomenological models based on the insight gained from the experimental observation and numerical simulations.

Although there have been some progresses in microscale evaporation and boiling research in the recent years, it is still a great challenge to experimentally investigate the effect of different types of nanostructures on boiling/evaporation due to the complexity of physical phenomena at nanoscale. Experimental studies have showed that using nanostructure on flat surface provides significant enhancement in heat transfer coefficient and critical heat flux [12–14]. Therefore, the study of parameters affecting the evaporation and boiling on nanostructure is one of the attractive topics. Recently, the fast advancement of micro/nanofabrication technology enables us to manufacture different kinds of novel hierarchical nanopatterns on a flat surface. Therefore, new opportunities to purse more efficient enhanced structures for boiling heat transfer can be explored. Geometry and size of nanopatterns are two of the main factors affecting the behaviors of boiling and evaporation. Different shapes of nanostructures [15–17] such as nanocylinder, nanosphere, mushroom-like, Y-shaped Nanorods, nanowire, and nanocone, can be manufactured for different applications. However, a deep understanding of physical phenomena during boiling of a liquid on different kinds of complicated nanostructures using experimental methods is still one of the challenging topics in nanoscale heat transfer.

In order to understand the heat transfer behavior in boiling, researchers depend heavily on computer simulation. Atomistic simulations, such as Non-Equilibrium Molecular Dynamics (NEMD) simulation, are playing increasingly important roles in investigations of complex and highly non-equilibrium processes such as evaporation/boiling at nanoscale surfaces. Recent studies involving Molecular Dynamics (MD) simulation of evaporation and boiling are presented in Refs. [18–26]. Maruyama and Kimura [18] performed a quasi-steady non-equilibrium molecular

* Corresponding author.
E-mail address: zhangyu@missouri.edu (Y. Zhang).

0017-9310/ - see front matter © 2013 Elsevier Ltd. Open access under CC BY-NC-ND license.
http://dx.doi.org/10.1016/j.ijheatmasstransfer.2013.07.025

Nomenclature

r_{ij}	distance between molecules i and j (Å)
E_i	embedding energy of atom i (eV)
F_i	force of atom i (eV/Å)
m_i	mass of atom i (gr/mole)
a_i	acceleration of atom i (eV mole/gr Å)
v_i	velocity of atom i (Å/ps)
N	number of atoms
k_b	Boltzmann constant (eV/K)
t	time (ps)
T	temperature (K)
P	pressure (bar)
x	coordinate in x-direction
y	coordinate in y-direction
z	coordinate in z-direction

Greek symbols

ε	energy parameter of LJ potential (eV)
σ	length parameter of LJ potential (Å)
ϕ	short range potential energy (eV)
Φ	potential energy for Ar–Ar and Ar–metal (eV)
ρ	atomic electron density
Δt	time step (ps)

Subscripts

Ar	Argon
Al	Aluminum
Ag	Silver

dynamics simulation to measure the contact thermal resistance over the solid–liquid interface. The results showed that the temperature jump at solid–liquid interface increased sharply with decreasing surface wettability. Seyf and Zhang [19] analyzed the separation of argon films over surfaces with and without spherical nanostructures using MD simulation. Their results showed that argon layers nearest the surface overheated and underwent explosive boiling which caused separation of liquid from the surface and consequently formation of a liquid droplet for flat surface case and formation of several tiny liquid clusters for surfaces with nanostructures. Yi et al. [20] simulated the vaporization phenomenon of an ultra-thin layer (2 nm) of liquid argon on a platinum surface for two different superheat temperatures. Gu et al. [21] studied the explosive boiling of thin liquid-argon on a metal surface. For thin films with thickness below seven monolayers, the liquid argon completely is vaporized and dissolved into a mixture of small clusters, while for higher film thickness only the near-surface Ar layers were vaporized. Wu and Pan [22] investigated the evaporation of a thin liquid argon layer into vacuum using molecular dynamics simulation. The results demonstrated that the net evaporation rate of thin film in a closed system may be modeled by the balance of evaporation and condensation based on the Schrage model. Novak et al. [23] using molecular dynamics simulation studied the homogeneous and heterogeneous bubble nucleation. They observed higher nucleation rate for the heterogeneous cases compared to that of the homogenous cases. Maroo and Chung [24] studied the effect of nanochannel height and film thickness on thin film evaporation in a nanochannel. They showed that both evaporation and heat flux rates exponentially decreased with time. With increasing the height of nanochannel, both net heat and evaporation fluxes increase. Furthermore, the results showed that the Hamaker constant increases with an increase in vapor pressure. In a follow up work [25], they studied heat and mass transfer, as well as pressure variation, a nanoscale evaporating meniscus using MD simulation. They reported very high heat flux and evaporation rates as well as significant increases of pressure after formation of non-evaporating film. Yu and Wang [26] performed NEMD simulation to study the evaporation of the thin film, equilibrium vapor pressure as well as non-evaporating liquid layer in a nanoscale triple-phase system.

Recently, Morshed et al. [27] performed molecular dynamics simulation of boiling of thin film adsorbed on a metal substrate whose surface is structured by an array of cylindrical nanostructure. They used platinum as wall material and the Lennard–Jones potential for Pt–Pt interaction. The results showed that the nanostructure has significant effect on evaporation /boiling of the thin film. They found that liquid responded very quickly and evaporation rate increased with increasing height of the nanostructures. Although some works about the nonoscale evaporation and boiling have been carried out by using NEMD simulations (e.g., [27]), there is still a lack of systematic understanding of the impacts of nanostructures on the evaporation/boiling enhancement. To improve the understanding of boiling over nanostructured surface with a different shape of nanostructures, we present a more accurate NEMD simulation based on Embedded Atom Method (EAM) potential for a surface structured with an array of conical nanostructures with two different wall materials which has more applications (i.e., Al and Ag). Therefore the main novelties of our work are (i) for the first time we used conical shape nanostructures and study the boiling over them, (ii) using more accurate potential of solid–solid interaction, and (iii) study the effect of two more applied wall materials on boiling phenomena over nanostructured surface. To the best of the authors' knowledge, this is the first paper that analyzes the effect of nanocone array and metal type on explosive boiling of argon.

2. Simulation model

The simulation box is a cube with size of 7.2 nm (x) × 7.2 nm (y) × 80 nm (z), which contains liquid and vapor argon, as well as solid metal atoms as the wall material. Four equal-sized cone-like nanostructures were placed on a flat metallic surface. The base and top diameters of nanostructures are 0.25 nm and 1 nm, respectively. Fig. 1 shows the configurations of the nanostructure surfaces. The solid wall and nanostructures were represented by layers of face-centered cubic (FCC; 111) metal atom corresponding to densities of 10.5 g/cm^3 and 2.7 g/cm^3 for silver and aluminum, respectively. The liquid atoms initially placed on a FCC lattice corresponding to density of saturated liquid at the temperature of 90 K and the region above it was filled with vapor argon atoms. The thickness of liquid is constant for all simulations while the height of nanostructure varies from 2 to 5 nm. Periodic boundary conditions are applied on the x- and y- directions while the top boundary is elastic and adiabatic, i.e., the argon atoms are reflected back to the domain without any loss of momentum or kinetic energy. Nine layers of metal atoms were constructed to form the bottom wall, and different layers match with different functionalities. From the bottom to top, the first layer is fixed to avoid any migration of sample; the next two layers are set as heat source from which heat flux was generated; and the last six layers are set as solid walls through which heat is conducted to argon fluid. It is important to note that the lattice constant is different for aluminum and silver hence the number of atoms in the computational

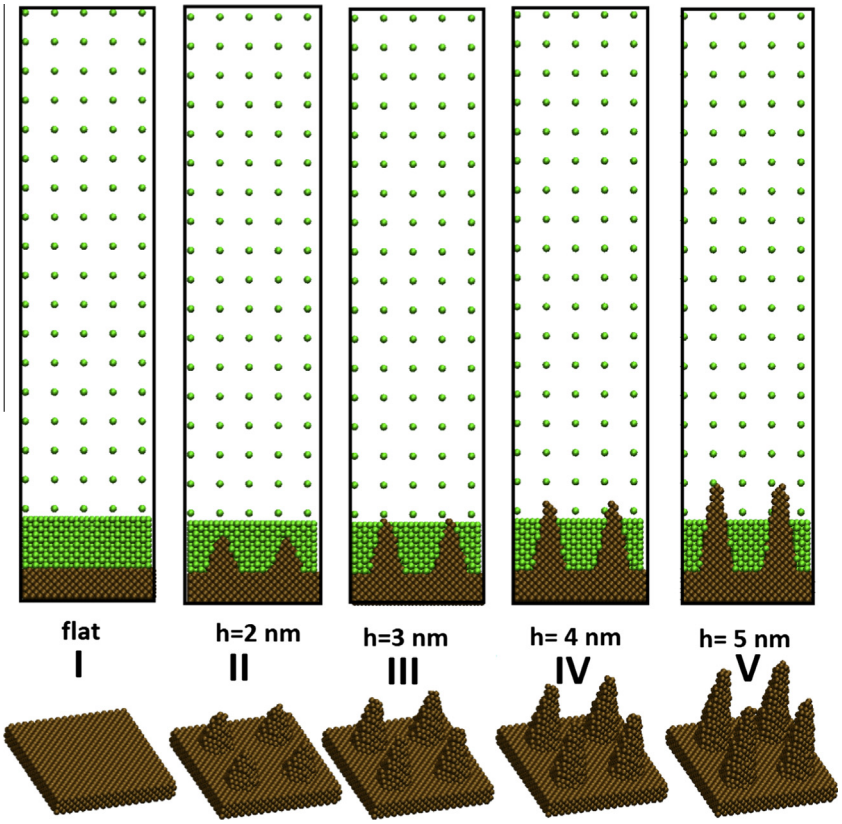

Fig. 1. Computational domain, initial atoms configuration and geometries of nanostructures.

domain is different for each wall material. The total number of atoms for cases with aluminum and silver as wall material is around 8896–10051 and 8884–10156, respectively, which correspond to different nanostructure.

For a MD simulation, the most important step is to choose an interatomic potential that describes the interaction between atoms. In this work, two different potentials are used. One is the embedded atom method (EAM) potential which takes the metallic boding into account and is more accurate in describing the interatomic interaction between metal or alloy atoms. The other one is the well-known Lennard–Jones (L–J) potential which matched the experimental data reasonably well for the property of liquid argon.

For the interaction of metal–metal atoms, the total energy E_i (for pure metal) of the atom i is given by [28]

$$E_i = F_i\left(\sum_{j\neq i}\rho_i(r_{ij})\right) + \frac{1}{2}\sum_{j\neq i}\varphi_{ij}(r_{ij}) \tag{1}$$

where E_i is the embedding energy of atom i and it is a function of the atomic electron density ρ, and φ is a short-range pair potential interaction between the atoms i and j. The interatomic interaction between argon–argon and argon–metal atoms are described by the well-known L–J potential

$$\Phi = 4\varepsilon\left[\left(\frac{\sigma}{r_{ij}}\right)^{12} - \left(\frac{\sigma}{r_{ij}}\right)^{6}\right] \tag{2}$$

where ε and σ are energy of interaction and equilibrium distance, and both of them depend on the type of the molecules. For interaction of metal–Argon atoms, the following Berthlot mixing rule [29,30] was used

$$\begin{aligned}\varepsilon_{\mathrm{Ar-metal}} &= \sqrt{\varepsilon_{\mathrm{Ar-Ar}}.\varepsilon_{\mathrm{metal-metal}}}\\ \sigma_{\mathrm{Ar-metal}} &= \frac{\sigma_{\mathrm{Ar-Ar}} + \sigma_{\mathrm{metal-metal}}}{2}\end{aligned} \tag{3}$$

where the L–J potential parameters for argon–argon and argon–metal are summarized in Table 1.

Calculation of the forces acting on atoms is the most time-consuming task in the MD simulation. When the distance between two atoms is greater than the cut-off distance, the interactive force between the two atoms equals zero so those atoms with distances longer than the cutoff distance should be excluded from the force calculation. In this study we used four different cut-off distances, i.e., $3\sigma_{\mathrm{Ar-Ar}}$, $3.5\sigma_{\mathrm{Ar-Ar}}$, $4\sigma_{\mathrm{Ar-Ar}}$, and $5\sigma_{\mathrm{Ar-Ar}}$ for surface (III) and compared the results with each others. We did not observe any difference between $4\sigma_{\mathrm{Ar-Ar}}$ and $5\sigma_{\mathrm{Ar-Ar}}$ hence we choosed $4\sigma_{\mathrm{Ar-Ar}}$ for all of the cases studied in this paper. The force of the interaction can be calculated from potential function as follows:

$$F_i = \begin{cases} -\nabla\Phi & \textit{for} \quad \mathrm{Ar{-}Ar}\ \textit{and}\ \mathrm{Ar{-}metal} \\ -\nabla E_i & \textit{for} \quad \mathrm{metal{-}metal} \end{cases} \tag{4}$$

The simulations start from an initial state that includes the initial positions and velocities of the argon and metal atoms. The velocities of the atoms are determined based on the constant system temperature, which is 90 K here. The relationship between the atom velocities and the system temperature is given by:

$$\frac{1}{N}\sum_{i=1}^{N}\frac{1}{2}m_i\mathbf{v}_i^2 = \frac{3}{2}k_bT \tag{5}$$

where m_i is the mass of the atom, N is the total number of atoms, and v_i is the velocity of the atom i. In order to obtain the position and velocities of the atoms at every time step, the equation of

Table 1
L–J potential parameters for metal–metal, argon–metal, lattice constant and mass of solid atoms for different metals [30].

	σ(Å)	ε(eV)	$\sigma_{Ar-metal}$(Å)	$\varepsilon_{Ar-metal}$ (eV)	Lattice constant (Å)	Mass (gr/mol)
Silver (Ag)	2.574	0.351	2.987	0.060486	4.090	107.86
Aluminum (Al)	2.551	0.408	2.9755	0.065213	4.050	26.98

motion need to be integrated. After calculation of force of interaction, the Newton's second law is used to determine the acceleration:

$$\mathbf{F}_i = m_i \mathbf{a}_i = m_i \frac{d^2 \mathbf{r}_i}{dt^2} \tag{6}$$

where $\mathbf{a}_i$ and $\mathbf{F}_i$ are the acceleration and force acting on atom i, respectively. Finally, the position and velocities can be obtained using Velocity–Verlet integration method:

$$\begin{aligned} \mathbf{r}_i(t+\Delta t) &= \mathbf{r}_i(t) + \Delta t \mathbf{v}_i(t) + \frac{\Delta t^2 \mathbf{a}_i(t)}{2} \\ \mathbf{v}_i(t+\Delta t/2) &= \mathbf{v}_i(t) + \frac{\Delta t \mathbf{a}_i(t)}{2} \\ \mathbf{v}_i(t+\Delta t) &= \mathbf{v}_i(t+\Delta t/2) + \frac{\Delta t \mathbf{a}_i(t+\Delta t)}{2} \end{aligned} \tag{7}$$

We compared the results of different time steps at 1 fs, 2.5 fs and 5 fs and did not observe any significant difference between the results hence for all cases the time of step of 5 fs was chosen. The simulation contains three different steps. Firstly, the entire system was set at uniform temperature of 90 K using equilibrium molecular dynamics under Langevin thermostat method for 500 ps (Stage I). Once the total energy in the simulation does not change anymore, the thermostat is removed and then for the fluid domain, the Langevin thermostat was changed into NVE ensemble; the system was run for 500 ps while the temperatures of both nanostructures and solid surface were still fixed at 90 K by the thermostat (Stage II). Finally, the temperature of solid wall was set at a higher temperature (270 K) using NVT time integration via Nose/Hoover thermostat and simulations were run for enough steps to achieve equilibrium (Stage III). Empirically, if the argon temperature, pressure and density as well as total energy of the system are stable during the subsequent NVE ensemble stage just after the first stage, the system can be treated as in the thermal equilibration state. In order to check whether the argon is in equilibrium state, we monitored the density, pressure and temperature as well as system total energy of argon during the equilibration period. Figs. 2–4 illustrate the variations of average argon temperature and system energy as well as pressure and number density of argon for flat cases. It can be seen that for both cases with different materials the temperature and pressure fluctuate around mean value of 90 K and 1.35 bar and the system mean energy is respectively −1.59 eV/atom and −1.63 eV/atom for silver and aluminum during equilibrium period. When metal wall temperature increases, the explosive boiling occurs in liquid film and the temperature and energy of system increases. The average system energy in the final 3 ns is about −1.755 eV/atom and −1.825 eV/atom for Ag and Al, respectively. Furthermore, the equilibrium density shown in Fig. 4 indicates that the system is indeed in thermal equilibrium.

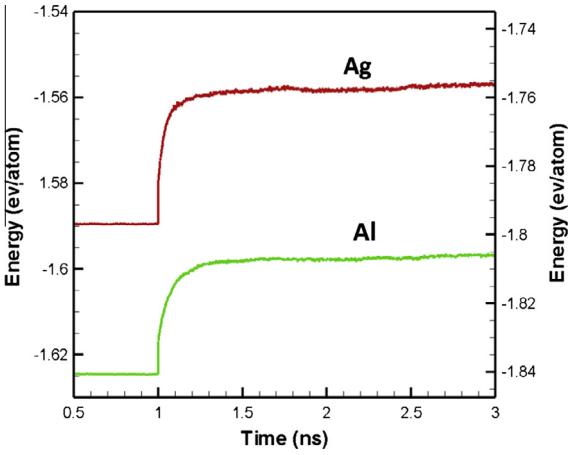

Fig. 2. Variation of average system energy with time.

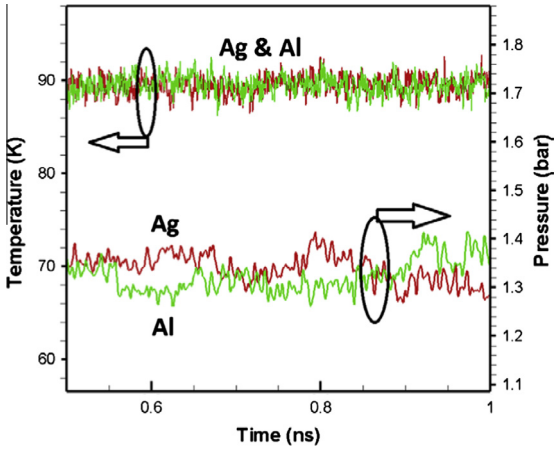

Fig. 3. Variation of average argon temperature and pressure with time.

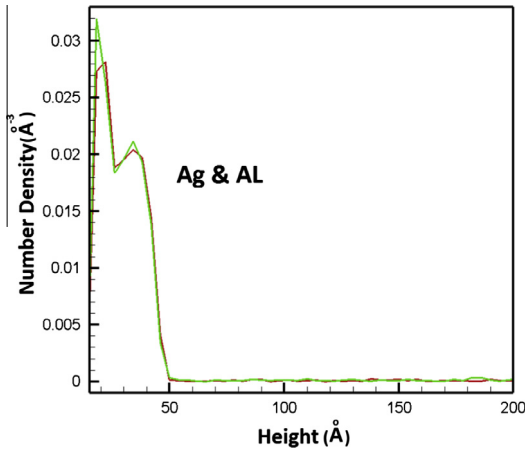

Fig. 4. Variation of equilibrium density with height of computational domain.

3. Results and discussions

3.1. Effect of nanostructure

To explicitly show the behavior of liquid during explosive boiling, we plot the x–z projection of the atomic configuration of the system for the silver wall and all cases with and without nanostructures in Figs. 5–9. Before the start of boiling, the interface between liquid argon and solid wall is clearly visible and the liquid argon shows a lower meniscus for surfaces IV and V due to the

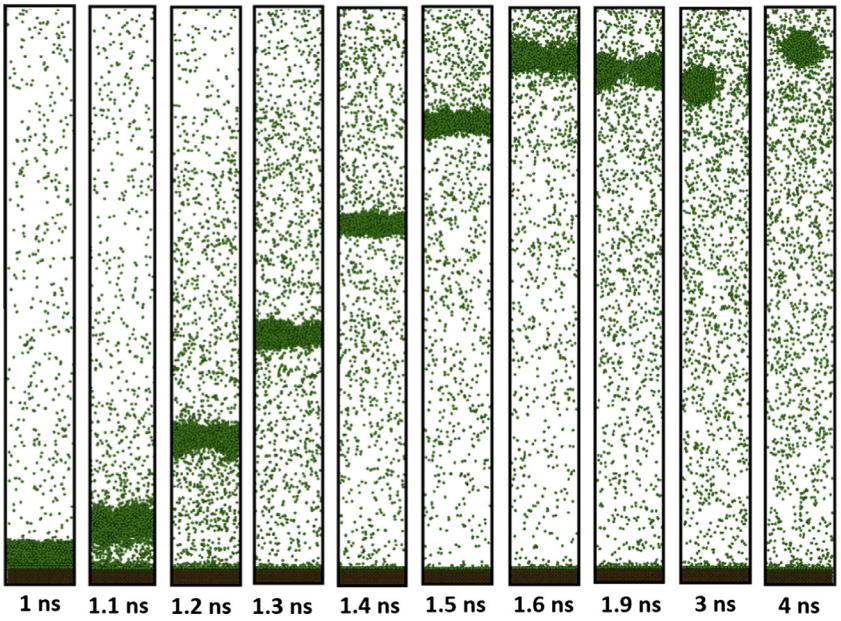

Fig. 5. Trajectories of atoms for surface I – silver case.

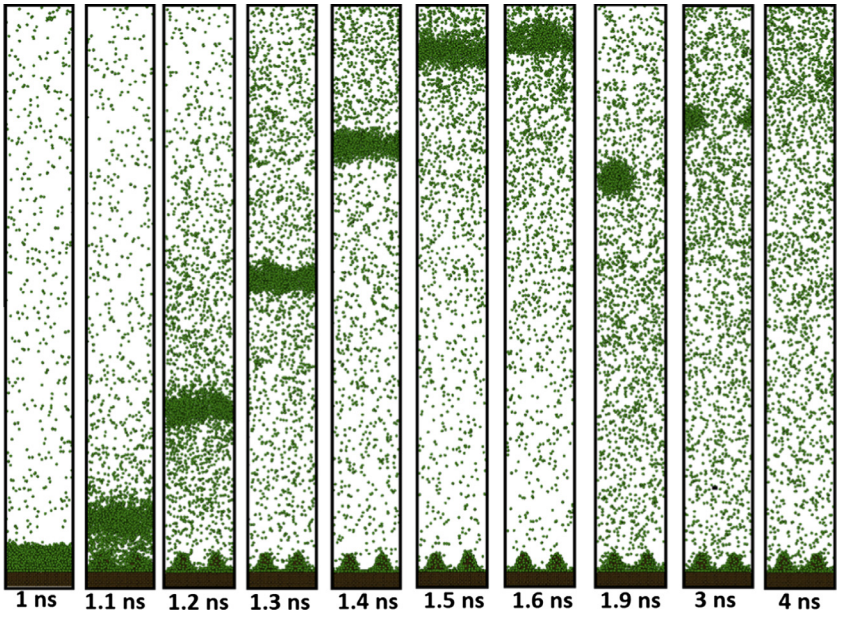

Fig. 6. Trajectories of atoms for surface II – silver case.

surface tension. It is clear that the system reaches to near equilibrium condition for all surfaces but equilibrium time varies for different nanostructure heights. For the case of flat surface, because of transfer of energy is only from the bottom, the evaporation last longer and the system reaches to steady state after a longer time; this means that faster evaporation on nanostructure than that on the flat surface because of lower solid–liquid interface resistance for nanostructured surfaces. At this point, it is worth mentioning that due to the quick rise of the wall temperature, liquid argon near the metallic wall reach the critical point temperature and vaporize while argons that is far away from the surface are still in the liquid phase. The resulting vaporized layer has high pressure, which pushes liquid above the surface away and consequently separates it from the solid wall. The separation of liquid cluster starts at around 1.37 ns and 1.50 ns for Cases I and V, respectively. Furthermore, for the case flat surface, the liquid layer above the surface separates from the solid as a large cluster of liquid while the size of liquid cluster differ for cases with nanostructures. With increasing size of nanostructures on the surface, the surface area of solid material in contact with liquid increases so that the temperature gradient in the liquid layer become less extensive than that of the flat surface. Therefore, a smaller cluster of liquid moves upward and the rest of liquid migrate as individual atoms in a well dispersed tiny cluster. It is worthy to note that due to larger heating area in the cases with larger nanostructures, the volume of liquid layer increases and the liquid moves upward so the separation starts from upper layer of liquid. The trends of the results in this section are consistent with the results obtained by Morshed et al. [27] for different geometry. Similar results were observed for cases with aluminum as wall materials.

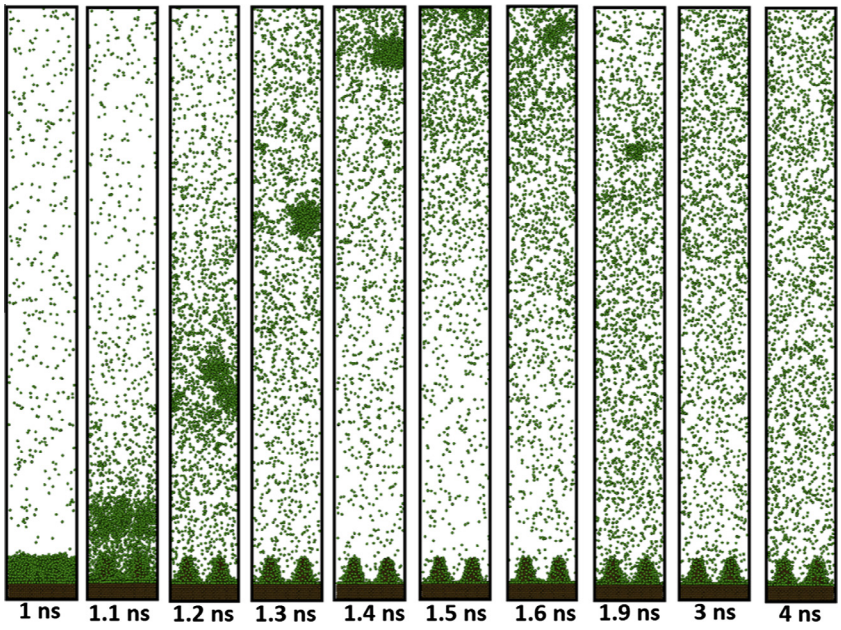

Fig. 7. Trajectories of atoms for surface III – silver case.

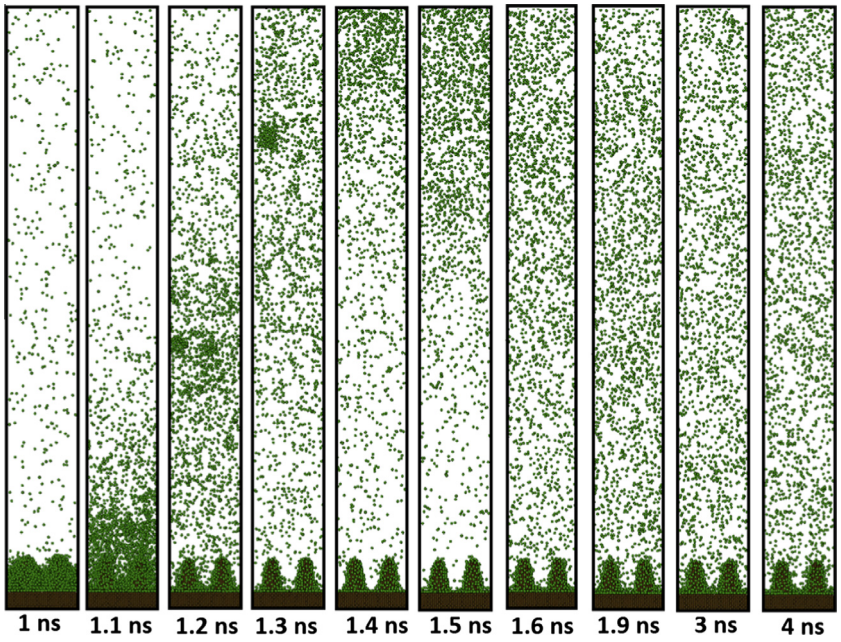

Fig. 8. Trajectories of atoms for surface IV – silver case.

The effects of cone-like nanostructure on the temperature and pressure histories of argon and wall material are shown in Figs. 10 and 11. For both wall materials, the walls respond very quickly to the temperature rise and reach the equilibrium in less than 50 ps. At the beginning of boiling stage, the argon temperature rises very rapidly and at some point it begins to decrease. As described earlier, at a specific time the liquid layers near the solid surface vaporize, which push the liquid upward and separate it from the solid as a large cluster of liquid. The temperature associated with separation of liquid from wall is called separation temperature. It is obvious that the generated vapor below liquid thin film and near the wall has a low density and it prevents energy flow from hot wall to the separated liquid above the vapor region. Therefore, as seen in a specific interval of time, the temperature of liquid falls and then starts to increases. Furthermore, the nanostructures lead to quicker energy transfer from solid wall to the liquid atoms and also higher argon temperature as results of increased solid–liquid interface area and interaction. Due to larger surface area of nanostructures compared with the flat surface, quick rise of wall temperature causes more energy transfer to the vapor atoms near the wall so the separation temperature increases due to the presence of cone-like nanostructures on the surface. Moreover, with increasing height of nanostructures, the argon temperature increases more and it reaches to equilibrium sooner. The equilibration times for cases with heights of 3–5 nm are around 8.5, 7.5 and 4.5 ns, respectively. Finally, it can be seen that for all

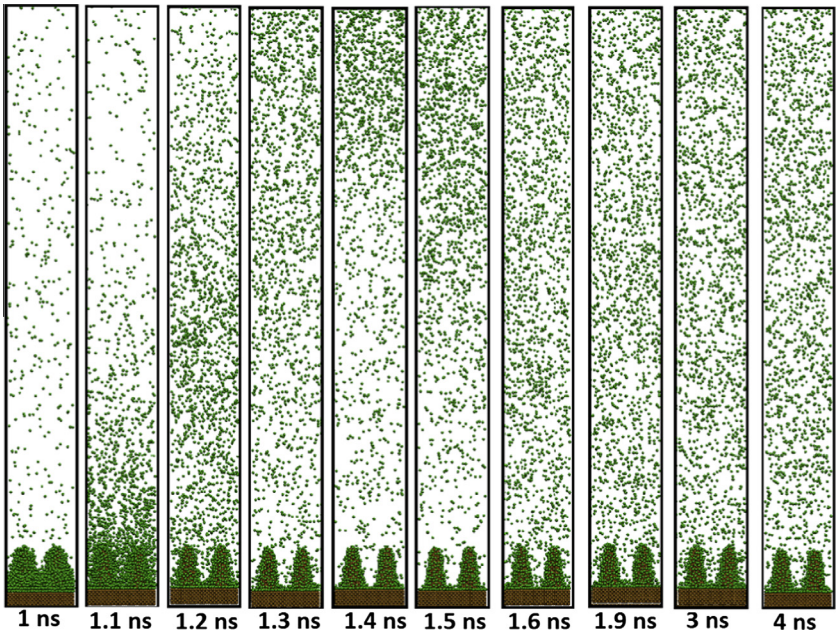

Fig. 9. Trajectories of atoms for surface V – silver case.

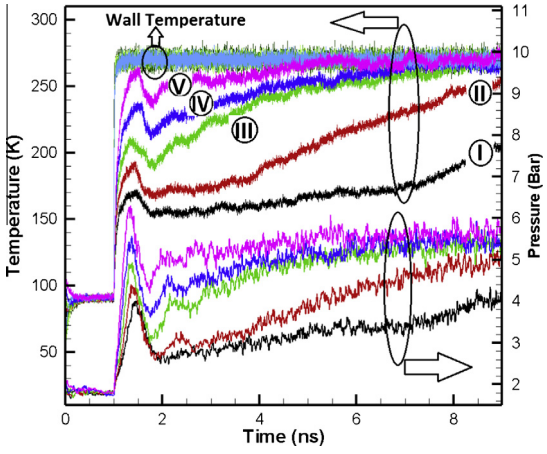

Fig. 10. Effect of aluminum nanostructure on temperature and pressure histories.

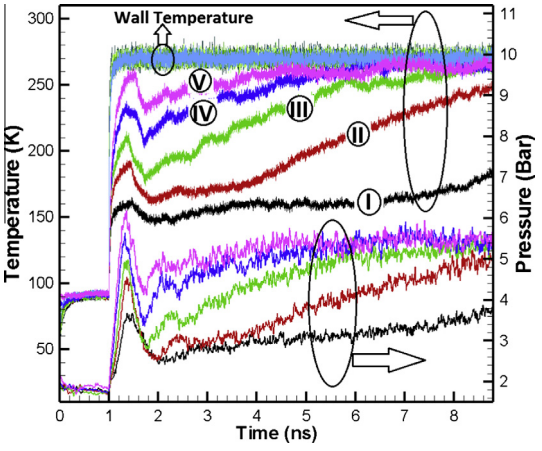

Fig. 11. Effect of silver nanostructure on temperature and pressure histories.

cases the pressures increase with time because they have the same trend as temperatures that increase in a fix volume. Moreover, for the cases with nanostructure, the pressure is higher than the one for the case of flat surface which is in agreement with trend of the temperature.

In order to calculate the number density in the z-direction, the computational domain along the z-direction is divided into 200 slices and the number of atoms in each slice is calculated to obtain the average density of the each slice. The effect of nanostructure on number density profile for two different time steps is shown in Figs. 12 and 13. The region of high density peaks appearing in the curves show the locations of floating liquid argon. It can be seen that for surfaces I–III there is a big liquid cluster in the computational domain that moves away from the surface, while for other surfaces there is not any significant peak in the curves which indicates the existence of tiny cluster in the system instead of large clusters.

For aluminum wall, at $t = 2.2$ ns, for the case of flat surface the peak value is 0.0115 and it is between 49 and 54 nm. For surface II the peak value is 0.0075 and is located between 57.5 and 62.5 nm. This means that with increasing height of nanostructures, the size of floating liquid argon decreases and it travels faster. For surfaces III–V, however, due to larger heat area and vaporization, there is not any large liquid cluster. As can be seen in all figures, due to strong intermolecular forces between solid and liquid, there is a high density region near the wall named non-evaporating layer. In this region the argon atoms near the surface distribute orderly in a solid-like state and show a crystal-like structure which will be described later in next section. Another important result is that the number density gradually flattens before and after each peak which show the disappearance of the vapor–liquid phase interface.

Figs. 14 and 15 illustrate the number of liquid and vapor atoms in the system during the simulation period. It is important to note that the change in number of vapor atoms represents the evaporation rate in the system. It can be seen that after the inception of boiling, the number of vapor molecules increases sharply and then it exhibits a linear growing trend; it finally becomes constant as the simulation time proceeds. The number of liquid molecules

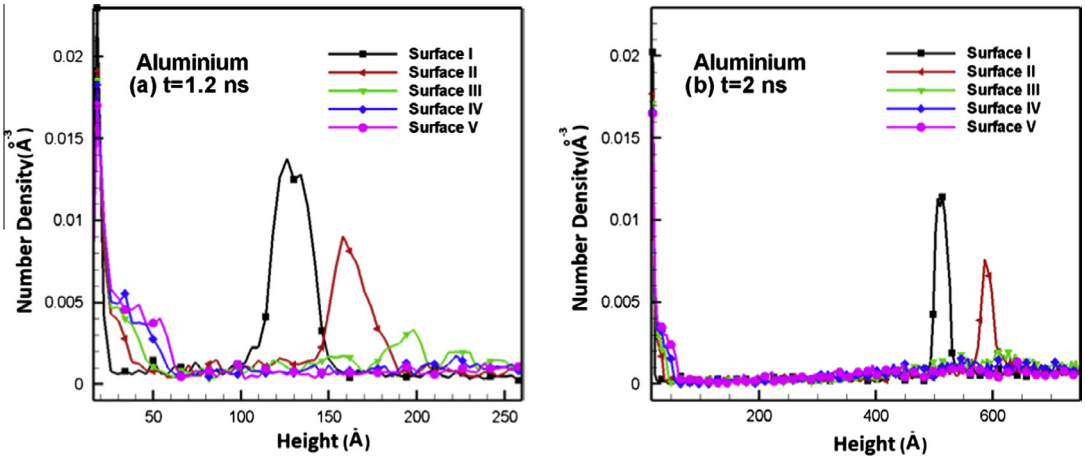

Fig. 12. Number density for aluminum: (a) $t = 1.2$ ns, and (b) $t = 2$ ns.

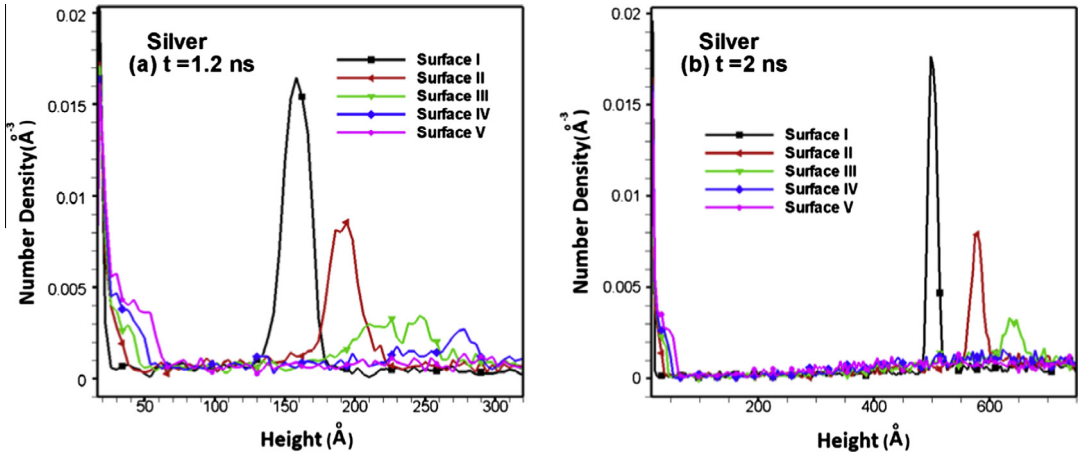

Fig. 13. Number density for silver: (a) $t = 1.2$ ns, (b) $t = 2$ ns.

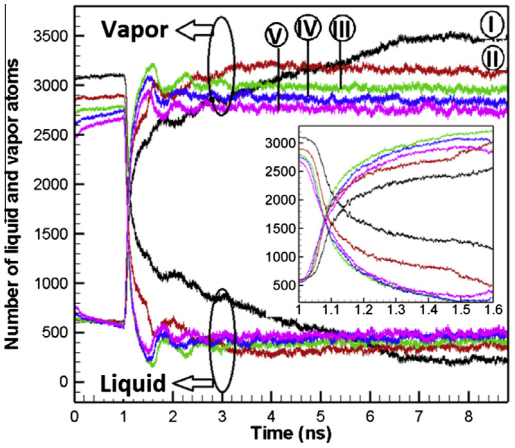

Fig. 14. Number of liquid and vapor atoms for aluminum case.

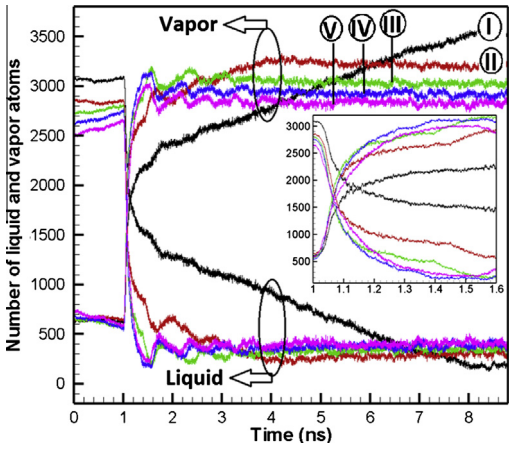

Fig. 15. Number of liquid and vapor atoms for silver case.

decreases after the beginning of boiling, has a linear decaying trend and finally reach to a constant value. The evaporation rate of all of nanostructured surfaces are almost constant after $t > 2.4$ ns while for flat surface it increases with time. This means that for nanostructured surfaces, there is not much significant evaporation after $t = 2.4$ ns because most of liquid atoms evaporated in the beginning of boiling process. In other words, for the nanostructured surfaces due to larger heating area and reduced thermal resistance at liquid–solid interface, very fast evaporation of liquid occurs in the beginning of boiling and the number of vapor and liquid atoms in the system reach to equilibrium very soon. For aluminum wall material at $t < 1.6$ ns, the evaporation rate of nanostructured surfaces is higher than that of the flat surface, while for 1.6 ns $< t <$ 6.7 ns flat surface shows higher evaporation rate. After

$t > 6.7$ ns there is not any significant evaporation in the system and the number of vapor and liquid atoms in the system reach to equilibrium. For silver case after $t > 1.6$ ns, the evaporation rate of flat plate case is higher than nanostructured surfaces and the number of vapor and liquid atoms in the system need longer time to equilibrate.

3.2. Effect of wall material

Figs. 16 and 17 show the argon temperature histories along with the pressure histories obtained for all nanostructure surfaces and both materials. It is worth to mention that the temperature gradient is large for liquid region while as seen in previous section the temperature of solid wall is almost flat; these correspond to low thermal conductivity of liquid argon and very high thermal conductivity of solid wall. Furthermore, consistent with the results presented in Figs. 10 and 11, there is a sudden rise and then fall of temperatures of liquid for all types of surfaces due to separation of liquid from the solid wall. For surfaces I–III, the effect of wall material on temperature history is significant; while for surfaces IV and V, there is a slight difference between argon temperatures for Al and Ag cases. Furthermore, the type of wall material does not have significant effect on equilibrium time while it has a slight effect on separation temperature in the flat case. For flat case, the separation temperature of the aluminum wall is higher than silver one.

The snapshots of the system for different wall materials (Fig. 18) show that in the concerned region of near the heating wall and nanostructures, the argon molecules distribute orderly in a solid-like state. A little further away the heating wall, the molecules move in a larger region. The further away, the more randomly molecules move. After first period of boiling, the liquid droplet in the cases with Ag wall travels faster than the one for Al case because silver has higher conductivity than that of aluminum. Here it is worth to note that due reduction of attractive forces between fluid and solid atoms with decreasing solid–liquid interactions, the mobility of the liquid atoms adjacent to the solid and consequently the driving force which is proportional to molecular mobility increases. Therefore, for the case of Ag surface because of lower liquid–solid interactions, the velocity of argon atoms near the solid wall increase more and hence the upward velocity of liquid droplet increases and the separation of droplet from the surface occur sooner for the case of silver compared to the case for aluminum. Study of the number density profiles for different wall materials is important because it gives an indication about the size and velocity of the liquid droplet and the thickness of the interface.

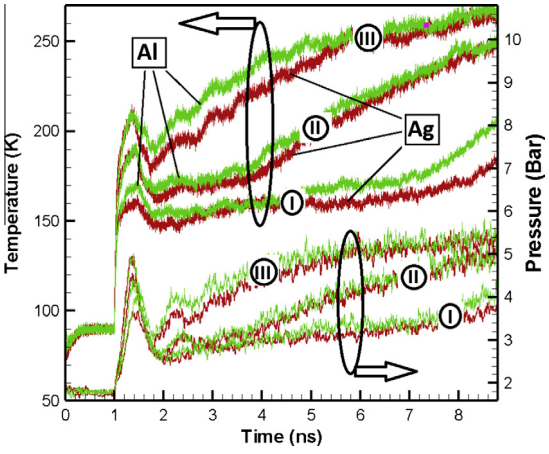

Fig. 16. Effect of wall material on temperature and pressure histories of surfaces I–III.

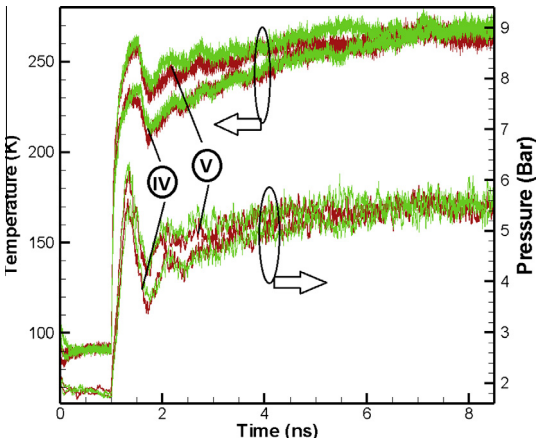

Fig. 17. Effect of wall material on temperature and pressure histories of surfaces IV and V.

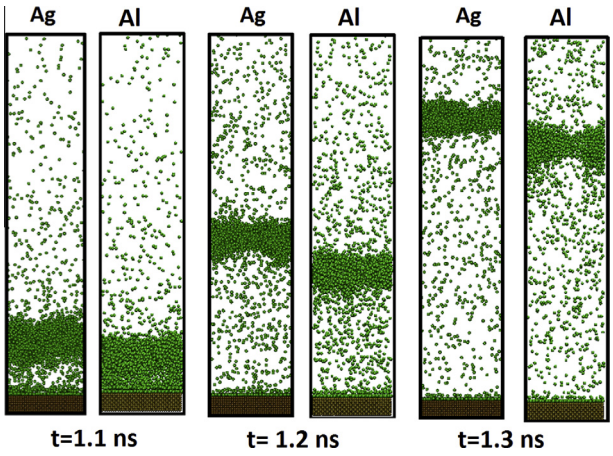

Fig. 18. Effect of wall material on Trajectory of atoms for surface I.

Figs. 19–21 shows the local number density as function of the height of computational domain for two time periods after onset of boiling ($t = 1.2$ and 2 ns) and for both materials. The local number density profiles show as four different regions. The first region is the non-evaporative region that is near the solid surface, the second region is the liquid phase with relatively high density, the third is the liquid–vapor interface, and the forth region is the vapor phase. For the aluminum case the thickness of non-evaporative region is greater than the one for silver due to the stronger attraction between aluminum and argon atoms. The local density shows some scattering in vapor region because of small number of particles in this region. As showed earlier in the very beginning of boiling when the liquid thin film is in contact with solid wall, the liquid droplet for the silver case travels faster than the one for aluminum case. This is due to higher thermal conductivity of silver in comparison with aluminum that causes faster transfer of heat inside the metallic wall and consequently to the liquid argon. Furthermore, it is clear that for silver case the size of liquid droplet is larger than the one for aluminum case; this can also be due to higher liquid–metal interaction energy in aluminum case which cause some of liquid atoms attach to the solid walls so smaller number of liquid can travel upward. For the surfaces with larger nanostructures the liquid film evaporates very fast and most of the computational domain is filled with vapor phase.

The effect of wall material on the numbers of vapor and liquid atoms for surfaces I and V is shown in Fig. 22. It can be seen that

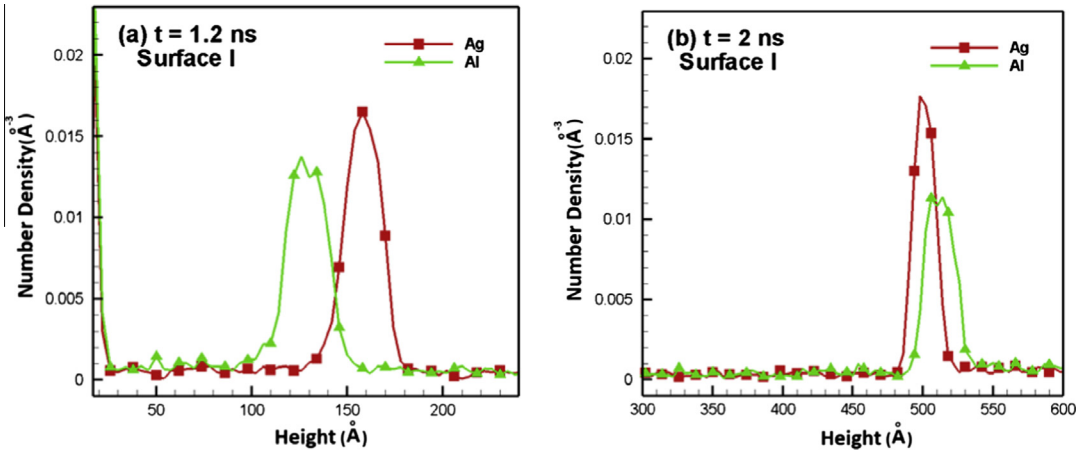

Fig. 19. Number density for surface I.

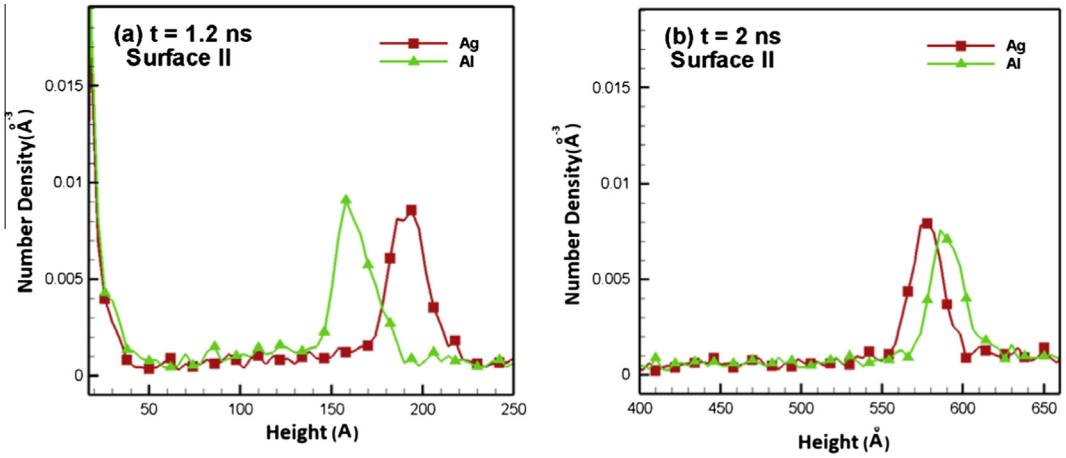

Fig. 20. Number density for surface II.

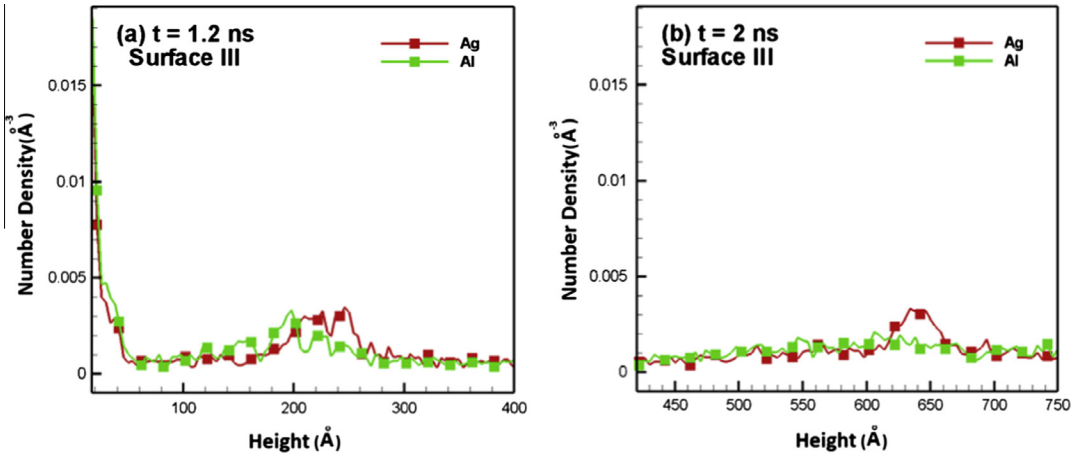

Fig. 21. Number density for surface III.

the numbers of vapor atoms for all the surfaces are constants after 2 ns and there is a region after start of boiling with high evaporation rate. It is worth to mention that very high evaporation exist at early stage of explosive boiling during the quick formation of non-evaporating film on solid wall; however, as the time that is required for its formation is only on the order of picosecond, the high flux rates are only sustained for a very short period of time. The results indicate that net evaporation numbers for the cases with aluminum is slightly higher than that of the silver case, and the non-evaporative number of atom for Al case is higher than Ag case due to larger solid–liquid interaction of Al–Ar compared with Ag–Ar. Furthermore, the previous studies on the liquid droplet on the surface [31,32] showed that the wettability of the surface is directly related to the depth of the integrated effective surface

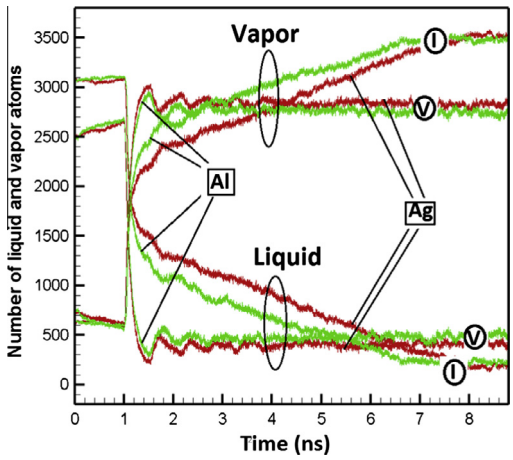

Fig. 22. Effect of wall material on number of liquid and vapor atoms.

potential ($\varepsilon_{\text{Argon-metal}}$) hence aluminum is more wettable for the liquid Argon due to its higher effective surface potential compared to silver. Therefore, for aluminum wall the argon cover the surface more and maintain its contact with solid surface better than the case with silver wall hence the transfer of energy from aluminum wall to Argon is higher and consequently the evaporation number increase more when using aluminum as wall material.

In all cases shortly after beginning of boiling, the evaporation on the hot wall stopped and an ultra-thin layer of argon atoms named non-evaporating layer [25,26] was left on surface (Fig. 23). Due to the strong intermolecular forces between the solid metal and the argon molecules, the argon near the flat solid wall and nanostructures showed a crystal-like structure with obvious periodicity. This layer contains atoms that are denser than the liquid layer but it looks sparser because the view direction in Fig. 23 is along the atom alignment such that the front atoms block the back ones. As was seen from Figs. 14 and 15, the number of non-evaporative molecules varies for different nanostructured surfaces. The number of non-evaporative molecules increases with increasing size of nanostructures because of large surface area attracts more liquid atoms. On the other hand, according to Table 1, the metal–argon interaction for aluminum and silver are nearly same so there is not any significant difference between the numbers of non-evaporating molecules for these two materials.

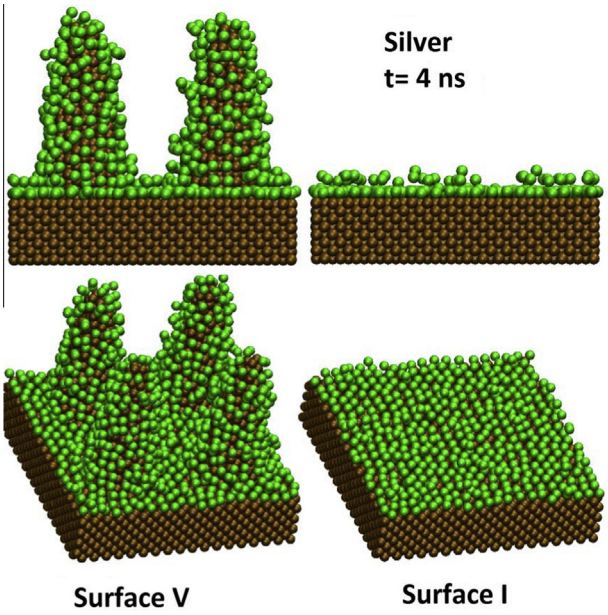

Fig. 23. Non-evaporative thin film region.

4. Conclusions

Explosive boiling of argon over cone-like nanostructures on a flat surface were investigated through nonequilibrium molecular dynamics simulation. Two wall materials and four cone-like nanostructures with different heights ranging from 2 to 5 nm were studied. While the interatomic potential between argon atoms is described using the Lennard Jones (L–J) potential, a more accurate embedded atom method (EAM) potential is used in describing the interatomic interaction between metal atoms. The results showed that the cone-like nanostructures enhance the heat transfer from solid to liquid, and increased the evaporation rate and argon temperature. However, the evaporation rate does not vary significantly with size of nano-textures when it is less or equal to thickness of the thin liquid film. It was observed that after inception of boiling liquid suddenly heated to a very high temperature and a cluster of liquid moves upward. The size of liquid droplet depends on the height of nanostructures, for surfaces I–III there is a big droplet in the system while for other surfaces there are some tiny clusters. The separation temperature associated with separation of liquid film from solid surface strongly depends on size of nanostructure but it is not sensitive to type of material. Furthermore, for all the cases studied, there are some non-evaporative argon atoms that are attached on the wall in the entire processes. For the cases with nanostructures the number of non-evaporative atoms is higher than the one for flat case; with increasing height of nanostructure, it increases more. Moreover, due to higher liquid–metal interaction for aluminum wall, the number of non-evaporative atoms is higher for aluminum wall.

Acknowledgement

Support for this work by the U.S. National Science Foundation under grant number CBET- 1066917 is gratefully acknowledged.

References

[1] V.P. Skripov, Metastable Liquids, Halsted, New York, 1974. p. 312.
[2] V.N. Alekseev, S.V. Egerev, K.A. Naugolnykh, O.B. Ovchinnikov, A.E. Pashin, O.B. Puchenkov, Acoustic diagnostics of transient interaction processes between optical radiation and a highly absorbing dielectric fluid, Sov. Phys. Acoust. 33 (1987) 561–565.
[3] A.A. Samokhin, In effect of laser radiation on absorbing condensed matter, in: A.V. Prokhorov (Ed.), Proceedings of the General Physics Institute USSR Academy of Sciences, 13, Nova Science, New York, 1990.
[4] A.A. Karabutov, A.P. Kubyshkin, V.Ya. Panchenko, Natalia B. Podymova, Dynamic shift of boiling point under laser action on metals, Kv Elektronika 22 (8) (1995) 820–824.
[5] H. Park, D. Kim, C. Grigoropoulos, A.C. Tam, Optical probing of the temperature transients during pulsed-laser induced boiling of liquids, Appl. Phys. Lett. 68 (1996) 596–598.
[6] H. Park, D. Kim, C. Grigoropoulos, A. Tam, Pressure generation and measurement in the rapid vaporization of water on a pulsed-laser-heated surface, J. Appl. Phys. 80 (1996) 4072–4081.
[7] D. Kim, M. Ye, C.P. Grigoropoulos, Pulsed laser-induced ablation of absorbing liquids and acoustic-transient generation, Appl. Phys. A Mater. Sci. Proc. 67 (2) (1998) 169–181.
[8] X. Xu, K. Song, Interface kinetics during pulsed laser ablation, Appl. Phys. A 69 (1999) S869–S873.
[9] J.H. Yoo, S.H. Jeong, R. Greif, R.E. Russo, Explosive change in crater properties during high power nanosecond laser ablation of silicon, J. Appl. Phys. 88 (2000) 1638–1650.
[10] E.T. Karim, Z. Lin, L.V. Zhigilei, Molecular dynamics study of femtosecond laser interactions with Cr targets, in: International symposium on high power laser ablation, 2012, pp. 280–293. DOI: 10.1063/1.4739881.
[11] Y. Dou, L.V. Zhigilei, N. Winograd, B.J. Garrison, Explosive boiling of water films adjacent to heated surfaces: a microscopic description, J. Phys. Chem. A 105 (2001) 2748–2755.

[12] H.S. Ahn, V. Sathyamurthi, D. Banerjee, Pool boiling experiments on a vano-structured surface, IEEE Trans. Compon. Packag. Technol. 32 (2009) 156–165.
[13] L. Chen, Z. Wang, P.I. Wang, Y. Peles, N. Koratkar, G.P. Peterson, Nanostructured copper interfaces for enhanced boiling, Small 4 (8) (2008) 1084–1088.
[14] R. Chen, M. Lu, V. Sninivasan, Z. Wang, H.H. Cho, A. Majumdar, Nanowires for enhanced boiling heat transfer, Nano Lett. 9 (2) (2009) 549–553.
[15] Jia Zhu, Zongfu Yu, Shanhui Fan, Yi Cui, Nanostructured photon management for high performance solar cells, Mater. Sci. Eng. R70 (2010) 330–340.
[16] Jian Wang, Hanchen Huang, S.V. Kesapragada, Daniel Gall, Growth of Y-Shaped nanorods through physical vapor deposition, Nano Lett. 5 (12) (2005) 2505–2508.
[17] Y.-W. Su, C.-S. Wu, C.-C. Chen, C.-D. Chen, Fabrication of two-dimensional arrays of CdSe pillars using E-Beam lithography and electrochemical deposition, Adv. Mater. 15 (1) (2003) 49–51.
[18] S. Maruyama, T. Kimura, A study on thermal resistance over a solid-liquid interface by the molecular dynamics method, Therm. Sci. Eng. 7 (1) (1999) 63–68.
[19] H.R. Seyf, Y. Zhang, Molecular dynamics simulation of normal and explosive boiling on nanostructured surface, J. Heat Transfer (2013), http://dx.doi.org/10.1115/1.4024668.
[20] P. Yi, D. Poulikakos, J. Walther, G. Yadigaroglu, Molecular dynamics simulation of vaporization of an ultra-thin liquid argon layer on a surface, Int. J. Heat Mass Transfer 45 (2002) 2087–2100.
[21] X. Gu, H.M. Urbassek, Atomic dynamics of explosive boiling of liquid-argon films, Appl. Phys. B 81 (2005) 675–679.
[22] Y.W. Wu, C. Pan, Molecular dynamics simulation of thin film evaporation of Lennard–Jones liquid, Nanoscale Microscale Thermophys. Eng. 10 (2006) 157–170.
[23] B.R. Novak, E.J. Maginn, M.J. McCready, Comparison of heterogeneous and homogeneous bubble nucleation using molecular simulations, Phys. Rev. B 75 (2007) 085413. p. 11.
[24] SC. Maroo, J.N. Chung, Nanoscale liquid–vapor phase-change physics in nonevaporating region at the three-phase contact line, J. Appl. Phys. 106 (6) (2009) 064911. p. 7.
[25] S.C. Maroo, J.N. Chung, Heat transfer characteristics and pressure variation in a nanoscale evaporating meniscus, Int. J. Heat Mass Transfer 53 (2010) 3335–3345.
[26] J. Yu, H. Wang, A molecular dynamics investigation on evaporation of thin liquid films, Int. J. Heat Mass Transfer 55 (2012) 1218–1225.
[27] A.K.M.M. Morshed, T.C. Paul, J.A. Khan, Effect of nanostructures on evaporation and explosive boiling of thin liquid films: a molecular dynamics study, Appl. Phys. A 105 (2011) 445–451.
[28] MS. Daw, M.I. Baskes, Embedded-atom method: derivation and application to impurities, surfaces, and other defects in metals, Phys. Rev. B 29 (12) (1984) 6443–6453.
[29] G. Nagayama, M. Kawagoe, T. Tsuruta, Molecular dynamics simulations of interfacial heat and mass transfer at nanostructured surface, in: Proceedings of the International Conference on Integration and Commercialization of Micro and Nanosystems (MNC) 21410, 2007, pp. 1–10.
[30] P.M. Agrawal, B.M. Rice, D.L. Thompson, Predicting trends in rate parameters for self-diffusion on FCC metal surfaces, Surf. Sci. 515 (2005) 21–35.
[31] S. Matsumoto, S. Maruyama, H. Saruwatari, A molecular dynamics simulation of a liquid droplet on a solid surface, in: Proc ASME/JSME Thermal Engineering Joint Conf., Maui, 1995, pp. 557–562.
[32] S. Maruyama, T. Kurashige, S. Matsumoto, Y. Yamaguchi, T. Kimura, Liquid droplet in contact with a solid surface, Microscale Thermophys. Eng. 2–1 (1998) 49–62.